



Cite this: *Soft Matter*, 2022, 18, 455

Drag force of polyethyleneglycol in flows of polymer solutions measured using a scanning probe microscope†

Ruri Hidema, * Ken-ya Fujito and Hiroshi Suzuki 

The drag force of polyethyleneglycol thiol (mPEG–SH) attached to a cantilever probe in the flows of glycerol and polyethyleneglycol (PEG) solutions was measured. The effects of the molecular weights of mPEG–SH, solute, and molecular weights of PEGs in the flows on the drag force were investigated. The drag force of mPEG–SH with any molecular weight in the flows of glycerol solutions was described well by the stem and ellipsoidal-flower model proposed in a previous study. However, the drag force further increased in the flow of the PEG solutions. To describe the increment, an assumption of polymer entanglement with mPEG–SH attached to the probe in the flow was employed. The modified stem and ellipsoidal-flower model that employed polymer entanglements fit well to the drag force of mPEG–SH with any molecular weight in the flow of the polymer solution.

Received 9th September 2021,
Accepted 2nd December 2021

DOI: 10.1039/d1sm01305j

rsc.li/soft-matter-journal

1. Introduction

The deformation of flexible polymers in fluids causes non-Newtonian fluid behavior of dilute polymer solutions, such as drag reduction,^{1–4} elastic instability,^{5,6} and sudden increase in extensional viscosity. These characteristic behaviors are caused by the extension of polymers in the fluids, which affects the dynamics of the fluids. For instance, in the drag reduction phenomenon, extended polymers affect the vortex generation in the buffer layer, which modifies the energy transfer in the turbulent flow.^{1,2} Elastic instability is enhanced by polymer entanglements owing to polymer extension.⁶ These complex phenomena need to be elucidated for related industrial applications, as well as for the fundamental polymer dynamics. However, it is difficult to observe the polymer behavior in fluids directly and predict the interaction with inherent fluid motion. Conventional experimental techniques obtain averaged quantities of polymers in fluids, which are usually sufficiently complex.

The extension of deoxyribonucleic acid (DNA) as a giant polymer in shear or extensional flow has been used to explain polymer dynamics in fluids.⁷ Perkins *et al.*⁸ and Smith *et al.*⁹ conducted pioneering work visualizing DNA extension in shear and extensional flow. Their work inspired single-molecule

science in flows, which shows the heterogeneity of individual chains.^{8,9} The observation of DNA extension in microfluidic devices has become increasingly important because of the great interest in biophysical and genomic applications. Many types of microfluidic device have been developed to stretch DNA,¹⁰ such as an optimized cross slot and hyperbolic microchannel,^{11–14} a microfluidic device with a micropillar array,^{15,16} and an extensional microfluidic device with obstacles for electrophoretic stretching.^{17,18} These devices are used to investigate the mechanical properties of DNA under homogeneous straining flow.

Observing the extension of a tethered polymer in a resting solution reveals the mechanical properties of a single polymer. The experimental technique known as “nanofishing” using an atomic force microscope^{19–25} and a method using optical tweezers together with single molecule analysis²⁶ are utilized to obtain a force–extension curve of a tethered single polymer in a resting solution. The force–extension curve obtained by this method can be analyzed using the freely jointed chain (FJC) and worm-like chain (WLC) models to elucidate the entropic and enthalpic elasticity of a single chain. The FJC model describes a single, isolated, flexible polymer chain without long-range interactions. The WLC model describes a polymer chain with intermediate behavior between a rigid rod and a flexible coil.^{19,25,27,28} Therefore, these models are useful for quantifying the interaction between polymers and solvents.²⁹ The force–extension curve was also effective in revealing the conformational change of a single polymer chain, such as the unfolding of proteins,^{30,31} the elasticity switch of single photochromic macromolecules,³² and the mechanical stability of proteins during chemical reactions.³³

Department of Chemical Science and Engineering, Kobe University, Kobe 657-8501, Japan. E-mail: hidema@port.kobe-u.ac.jp

† Electronic supplementary information (ESI) available: Details of the physical properties of the sample solutions, an example of the original experimental data, and verification of the experiments. See DOI: 10.1039/d1sm01305j

Tethered polymer dynamics in a flow have also been an important topic for several decades, as seen in the pioneering works of Perkins *et al.*³⁴ and Marko and Siggia.³⁵ This is because the tethered polymer conformation in a flow is related to many topics, such as biophysical and genomic applications,³⁶ lubrication of grafted polymers on a surface,^{37,38} and the fundamental polymer dynamics that induce non-Newtonian fluid properties.^{39–41} Visualization of tethered DNA in flows derives precise information about the polymer conformation; therefore, tethered DNA stretching in flows was observed to better understand the model describing the extension.^{35,42–44} DNA extension is affected by flow velocity, elasticity, and relaxation processes.

The pioneering theoretical work on the stretching of tethered polymer chains under flows and sequential works were proposed by Brochard-Wyart and coworkers.^{45–49} They investigated the conformation of polymer chains subjected to uniform flow. Chain elongation starts when the frictional force on a blob overcomes the thermal agitation of the polymer.

Because the Stokes friction force depends on the velocity around the blob, the confirmation depends on the velocity of the flow. Brochard-Wyart *et al.*⁴⁹ proposed an index (φ) to predict polymer conformation. The index φ is described as $\varphi = fl_{\text{po}}/k_{\text{B}}T$, where f is the uniform tension force applied to the polymer, l_{op} is the unperturbed persistent length, k_{B} is Boltzmann's constant, and T is the temperature. When φ is greater than 1, the polymer is in a taut regime. When φ is less than 1, the polymer conformation varies following the unperturbed state, trumpet regime, and stem-and-flower regime with increasing flow velocity. Moreover, the trumpet regime occurs only for a very limited range of velocities;⁴⁷ thus, the polymers are likely to be in the stem-and-flower regime under uniform flow. The stem-and-flower regime was experimentally confirmed by Fisher *et al.* through visualizing the DNA relaxation dynamics.⁴³ In their work, the polymer deformation predicted by calculation φ was also confirmed.⁴³

The extension of the polymer is affected by the tension force on the polymer owing to entropic elasticity. The chain tension increases from the free end to the attached end. Thus, in the case of the stem-and-flower regime, the steady polymer conformation was derived by the balance of the force pulling the coil portion at the free end and the Stokes friction of this portion.⁴⁷ Rzehak *et al.* conducted a more detailed numerical simulation of the deformation of a tethered polymer in a uniform flow.⁵⁰ They calculated the distribution of the free ends of a tethered polymer by considering the excluded volume and hydrodynamic interactions. They predicted the tethered polymer conformation and calculated the total drag force exerted on the polymer by external flow.

As described above, a large number of nanofishing microfluidics experiments and numerical studies have been performed to investigate polymer conformations in a solution or flow based on the mechanical properties and drag force. However, experiments in which the drag force of polymers, especially synthetic polymers, was measured directly are few. In a previous study, a method combining a scanning probe

microscope (SPM) and a flow channel was proposed to measure the drag force caused by a synthetic polymer.⁵¹ The drag force of polyethyleneglycol (PEG) was measured in flows of several viscosities, and it was confirmed by calculating the drag force of the polymers, assuming the polymer conformation as a stem and ellipsoidal-flower shape. The model and the calculation were simple; however, the model successfully explained the drag force obtained experimentally. In the present study, the drag force of PEG with several molecular weights was measured, and the model was tested on the results. Furthermore, the drag force was measured in the flows of the polymer solutions. In these experiments, the drag forces of polymers that were affected by the polymer–fluid and polymer–polymer interactions were directly measured. Such an interaction in a boundary layer in flows is important for characterizing non-Newtonian fluids.

The remainder of this article is organized as follows. In Section 2, the materials and experimental setup used in this study are summarized. In Section 3, the force measured by the experiments is described, and the validity of the experiments is verified. Then, the stem and ellipsoidal-flower models are adopted for the results. To describe the drag force of polymers in the flow of the polymer solution, polymer entanglements in the flow are considered. The main conclusions are summarized in Section 4.

2. Experimental

2.1 Material and rheological property measurements

Glycerol (FUJIFILM Wako Pure Chem. Corp.) and PEG (FUJIFILM Wako Pure Chem. Corp.) solutions were prepared in a wide range of concentrations, as shown in Table S1 (ESI†). The molecular weights of PEG were varied as 10k (PEG10k), 20k (PEG20k), and 35k (PEG35k). The concentrations of these solutions were adjusted to obtain similar viscosities at each level. The viscosities of the sample solutions were measured using a rheometer (MCR301: Anton Paar) with a cone-plate device. All PEG solutions used in the drag force measurements show Newtonian viscosity, that is, the viscosities of PEG solutions were constant at all shear rates. To quantify the solution properties, the overlap and entanglement concentrations were determined by zero-shear specific viscosity; as is shown in Fig. S1 (ESI†). The concentration of PEG solutions used in the drag force measurements are in a dilute or semi-dilute unentangled regime. The entanglement molecular weight of PEG is about 2000. The density of each solution was measured using a densimeter.

To attach polymers to the cantilever probe, methoxy polyethyleneglycol thiol (mPEG–SH), which has a free thiol group at one end, was dissolved in pure water at a concentration of 1 wt%. The thiol group was bonded to a gold-coated cantilever probe, as described later. The molecular weights of mPEG–SH were 10k (mPEG–SH 10k, Laysan Bio Inc.), 20k (mPEG–SH20k, Laysan Bio Inc.), and 40k (mPEG–SH40k, Biochempeg Scientific).

Here, a gold-coated cantilever probe with a V-shaped tip (Biolever, BL-RC150VB-C1, B lever, Olympus) was used. Geometrically, it is a hollow pyramid that is vertically sliced

in half, with a sharpened apex. The convex surface of the probe is fully coated with gold. The front view of the probe from the convex side, is a triangle with a $12\ \mu\text{m}$ base and $7\ \mu\text{m}$ height. An upside-down image of the cantilever illustrating the V-shaped probe and the front view of the probe are shown in Fig. 6(b)–(d). The spring constant of the probe is about $6\ \text{pN nm}^{-1}$, which was provided by Olympus Corp. We assumed that the spring constant was not influenced by grafted polymers. For the measurement calibration, the diffraction signal (DS) was measured in each experiment. DS is a conversion coefficient between the cantilever displacement and the sensor signal. The signal detected by the voltage was converted to the force using the DS value and the spring constant.

2.2 Experimental procedure to measure drag force

The experimental system for measuring the drag force of polymers combines several apparatuses. The main apparatus used was an SPM (Innova, Bruker Nano). A small channel was attached to the sample stage of the SPM and connected to two syringes by tubing. A syringe was filled with sample solutions, and the flow rates of the inlet sample solutions were controlled by two syringe drivers. The flow rates were varied from 2 to $5\ \text{mL min}^{-1}$. A whole image representation of the flow channel is shown in Fig. 1(a), whereas Fig. 1(b) and (c) show the lateral view of the channel. A small stainless steel piece was sunk in the channel to stabilize the flow, producing a uniform flow at the inlet and a fully developed flow around the cantilever probe.⁵¹ The cover glass shown in Fig. 1(b) was used only when the velocity profiles at the test position was measured. The cover glass helps to achieve a similar flow profile to the flow in the channel covered by the microcell holding the cantilever, as shown in Fig. 1(c). To measure the velocity profile in the channel, the center line of the channel was illuminated by a laser sheet with a thickness of $1\ \text{mm}$. Polystyrene particles, with a diameter of $6.83\ \mu\text{m}$, were seeded in the sample solutions to calculate the velocity using the particle tracking velocimetry method (PTV). The velocity profiles at the test position normalized by the mean velocity are shown in Fig. 1(e). Here, the mean velocity was calculated by the flow rates divided by the cross-sectional area at the test position. The velocity profiles were compared to the theoretical velocity profile of the fully-developed laminar flow of Newtonian fluids in a duct, which confirms that the flow is fully developed.^{51,53}

The velocity profiles shown in Fig. 1(e) were obtained without the cantilever, which may be varied in the cantilever presence during the drag force measurement. However, we can assume the change in the velocity fields to be small because the equivalent diameter of the cantilever probe is less than 0.26% of the channel height, and its width is only 0.25% of the channel width. Therefore, we used the velocity at the height of $1.4\ \text{mm}$, at the test position, as the actual characteristic velocity.⁵¹

The cantilever was held by a microcell of the SPM, which was attached to a probe cartridge, as shown in Fig. 1(c), and the probe cartridge was inserted into the probe head. As shown in Fig. 1(c) and (d), the cantilever was held by the microcell at an angle θ of approximately 15° . The apex of the probe was placed

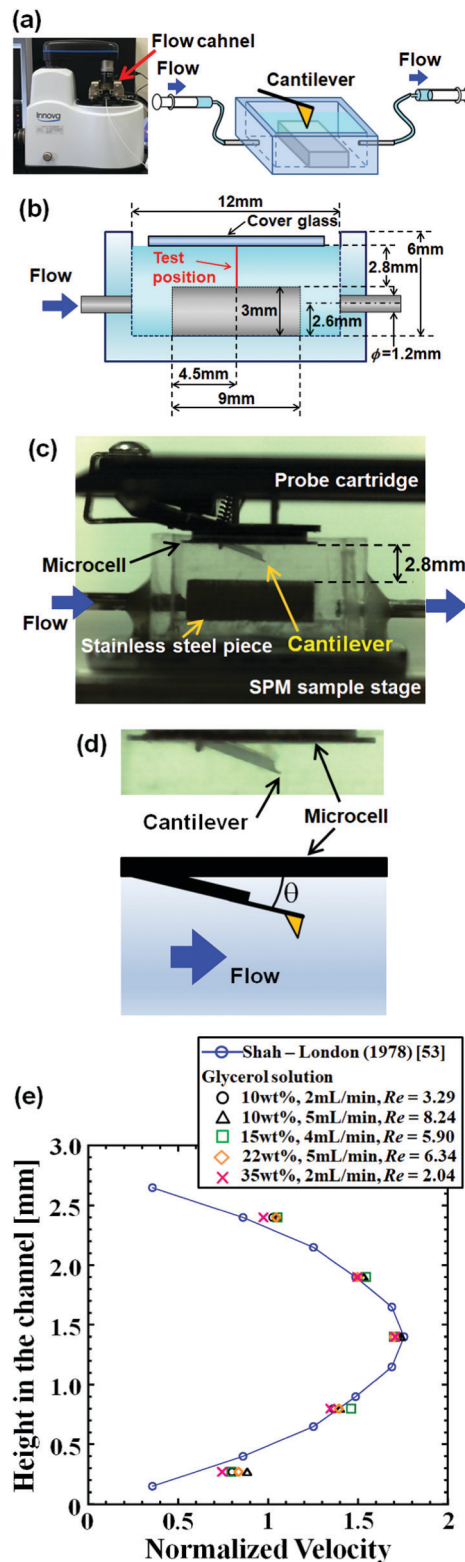


Fig. 1 Experimental system to measure the drag force applied to a cantilever in flows. (a) The hole image of the channel attached to the SPM. (b) The schematic of the lateral view of the channel. (c) The real image of the lateral view of the channel with a cantilever. (d) The cantilever was held with an angle of $\theta = 15^\circ$. (e) Normalized velocity profile for each glycerol solution at different flow rates.

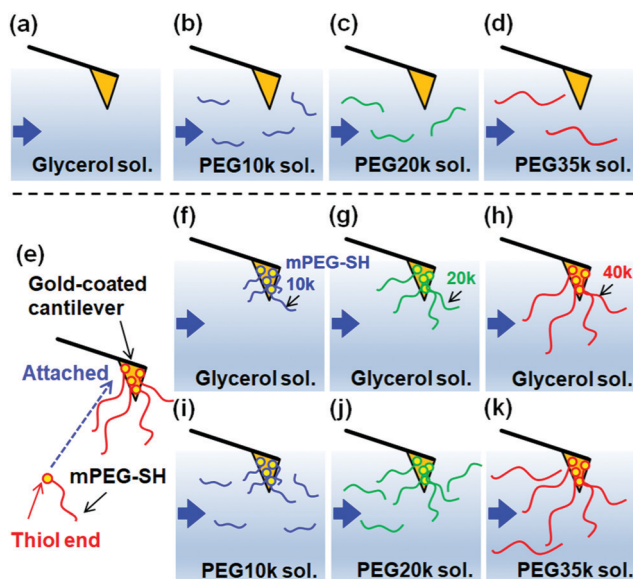


Fig. 2 Schematic of the experimental procedure. A cantilever with the original gold-coated probe was positioned in flowing solutions of (a) glycerol, (b) PEG10k, (c) 20k, and (d) 35k solutions. The cantilever was further immersed in mPEG-SH10k, 20k, and 40k solutions to attach the thiol end to the gold-coated probe (e). The mPEG-SH-bonded cantilever probe was further immersed in the flow of (f)–(h) glycerol and (i)–(k) PEG solutions.

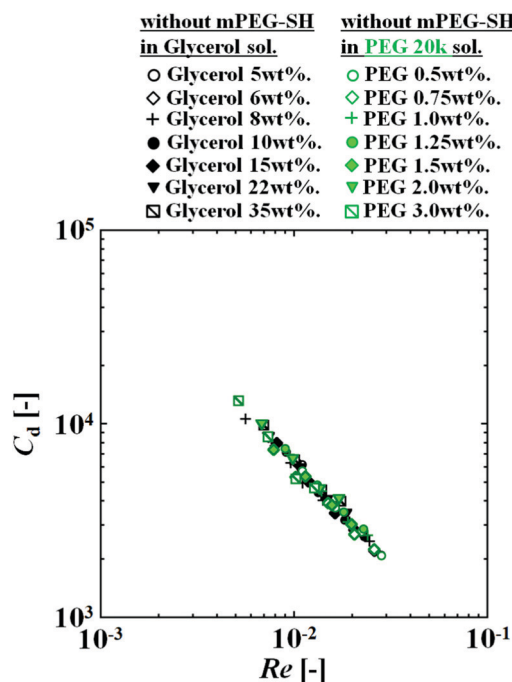


Fig. 3 C_d – Re plot for the naked cantilever probe in glycerol and PEG20k solutions.

in the middle of the channel, and the force applied to the cantilever in the flow was detected. The signal from the SPM was measured using an oscilloscope (WaveAce 1001, Teledyne LeCroy). The oscilloscope did not detect any force when the

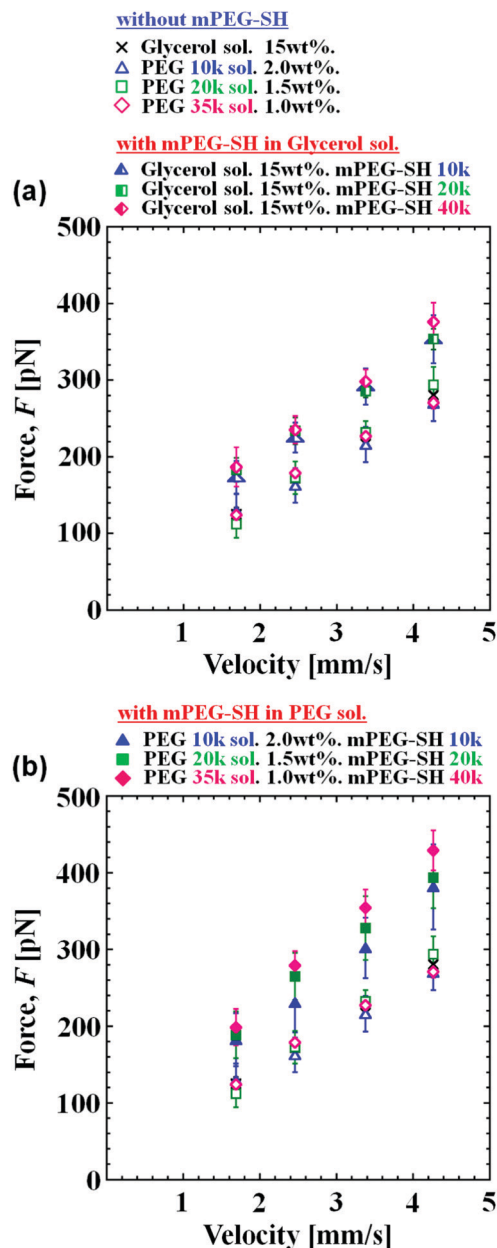


Fig. 4 (a) Comparison of the force measured by a naked cantilever in flowing glycerol and PEG solutions and that of the mPEG-SH-bonded cantilever in glycerol solutions. The molecular weights of mPEG-SH were varied. (b) The force measured for the several molecular weights of mPEG-SH-bonded cantilever in PEG solutions. The viscosities of the flowing glycerol and PEG solutions are similar, as shown in Table S1 (ESI[†]).

sample solution was at rest. However, when the sample solution flowed through the channel, the oscilloscope detected a drag force (Fig. S2, ESI[†]). The increase in the force measured by the probe was analyzed to study the polymer–fluid and polymer–polymer interactions.

The drag forces were measured under several conditions, as shown in Fig. 2. First, the originally gold-coated cantilever probe was used to measure the drag forces in flows of glycerol PEG10k, PEG20k, and PEG35k solutions—see Fig. 2(a)–(d).

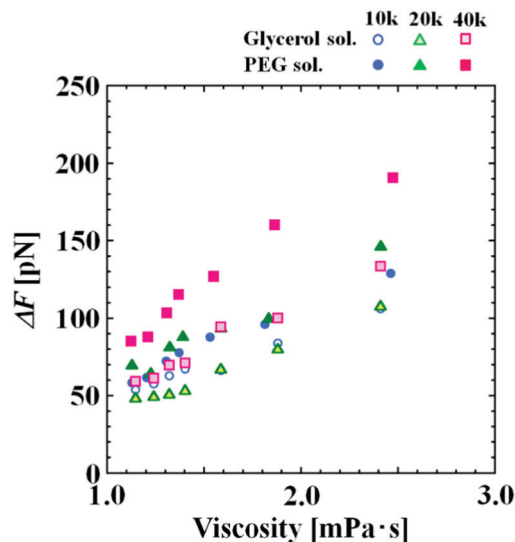


Fig. 5 Force difference, ΔF , affected by the viscosity of flows, the molecular weight of mPEG–SH attached to the cantilever probe, and that of PEGs in flows. The open symbols represent the comparison between (a) and (f)–(h) in Fig. 2. The solid symbols are represent the comparison between (b) and (i), (c) and (j), and (d) and (k) in Fig. 2, respectively.

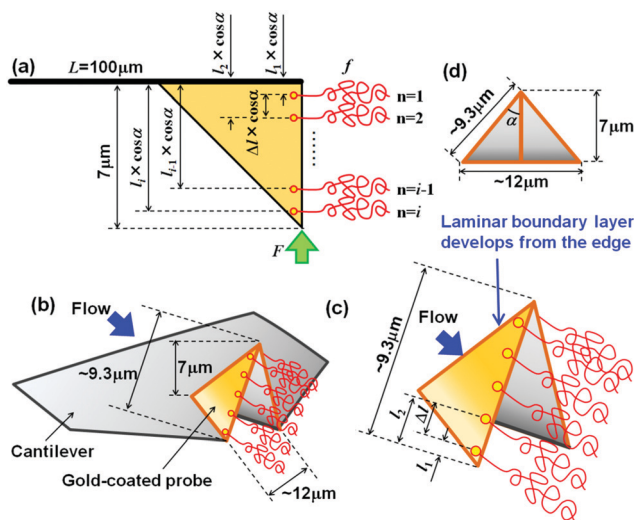


Fig. 6 (a) Lateral view of the cantilever with a gold-coated probe where the mPEG–SH attached, (b) upside-down image of the cantilever to illustrate the V-shaped probe, where mPEG–SH molecules attach to both its lateral sides, (c) close-up figure of the probe to indicate l_i and Δl along the edge, and the initial point of the laminar boundary layer development, and (d) close-up figure of the probe from the downstream view showing the apex angle.

The viscosities of these solutions were similar, allowing observation of the effects of solute and molecular weight of PEGs in the flows on the drag force. Subsequently, 1 wt% mPEG–SH10k, 20k, and 40k solutions were prepared and each mPEG–SH was attached to a gold-coated cantilever. The thiol group was attached to the gold-coated surface through coordinate bonding when the cantilever was immersed in the mPEG–

SH solution for 2 h, as shown in Fig. 2(e). The saturation of the bonding was confirmed by measurements using a quartz crystal microbalance (QCM922A, SEIKO EG&G CO.). After the bonding, the polymer-bonded cantilever was moved to the flow of glycerol and PEG solutions to detect an increase in the drag force because of the polymers attached to the cantilever—see Fig. 2(f)–(k). In the flow of glycerol solutions, the molecular weight of mPEG–SH attached to the cantilever probe is thought to affect the force detected by the polymer-bonded cantilever, as in Fig. 2(f)–(h). In the flows of PEG solutions, the polymer-bonded cantilever detected additional force resulting from the PEGs in the flow—see Fig. 2(i)–(k). Thus, the force measured by the polymer-bonded cantilever detects polymer–fluid and polymer–polymer interactions in flows.

3. Results and discussion

3.1 Force measurement in the flow and validity of the experiments

A cantilever with and without polymers was used to detect the drag force in a flow of several sample solutions. The force measured by a polymer-bonded cantilever was increased compared to that measured by a naked cantilever, which was attributable to the polymers attached to the cantilever. However, before discussing the contribution of polymers to the drag force, it is necessary to verify the validity of the experiments. Therefore, the drag coefficient, C_d , of the cantilever probe was calculated using the following expression.

$$C_d = \frac{F}{\frac{1}{2}\rho V^2 \pi \frac{d^2}{4}} \quad (1)$$

Here, F N is the force applied to the cantilever, ρ kg m^{-3} is the density of each solution, V m s^{-1} is the velocity at the location at the middle height at the test position shown in Fig. 1(b), and d m is the equivalent diameter of the probe. The front view presents an isosceles-triangular shape with a 12 μm base and 7 μm height with an apex angle of 2α °—see Fig. 6(d). Thus, the equivalent diameter d m of the probing area is 7.4 μm . Fig. 3 shows the C_d values found for the naked cantilever probe, plotted as a function of the Reynolds number, Re . In the figure, Re was calculated using the local velocity, V , and the equivalent diameter of the probe, d , as described in $Re = \rho V d / \eta$. As shown in Fig. 3, the C_d of a naked cantilever probe depends only on Re . The C_d value was not affected by the solute, such as glycerol or PEG20k, the concentration, or the solution viscosity. The C_d values of the naked cantilever probe measured in the PEG10k and PEG35k solutions are shown in Fig. S3 (ESI[†]), which are also a function of Re . C_d – Re is independent of the solution around the naked cantilever, verifying the validity of the measurements.

Fig. 4 shows the force detected by the naked and polymer-bonded cantilever in the flows of several solutions at several velocities. The force detected by a naked cantilever was not affected by the solutions, such as glycerol 15 wt%, PEG10k 2.0 wt%, PEG20k 1.5 wt%, and PEG35k 1.0 wt%—see Fig. 4(a). The viscosities of the solutions were almost the same.

Conversely, the detected force increased in the flow of the glycerol solution when mPEG-SH was attached to the cantilever probe. Furthermore, the force was slightly affected by the molecular weight of the mPEG-SH attached to the cantilever probe. The probe with mPEG-SH, having a larger molecular weight, detects a larger force, as in Fig. 4(a). In the case of the polymer-bonded cantilever in PEG solutions, the force was influenced by the molecular weight of mPEG-SH attached to the cantilever probe and that of the PEGs in the flow—see Fig. 4(b). The larger molecular weights of mPEG-SHs and PEGs increased the detected force. The force differences, ΔF pN, that is the increase in the detected force calculated as the difference between the forces measured by the polymer-bonded probe and by the naked probe are compared in Fig. 5. Here, the velocity around the cantilever was fixed at approximately $V = 3.14 \text{ mm s}^{-1}$, which corresponds to 4 mL min^{-1} , controlled by the syringe driver. The viscosity difference was caused by the concentration of each glycerol and PEG solution. In addition, ΔF was increased by increasing the viscosity of the flow. The ΔF measured in PEG solutions was higher than that in glycerol solutions, and ΔF was influenced by the molecular weight of mPEG-SH bonded to the cantilever probe and the molecular weight of the PEGs in the flows. These differences are considered to result from polymer–fluid and polymer–polymer interactions in the flows.

3.2 Polymer conformation and drag force caused by polymers

The increase in the detected force, ΔF , resulted from the mPEG-SH attached to the cantilever probe. Therefore, the drag force caused by mPEG-SH was calculated, which contributes to ΔF . To calculate the drag force of a single polymer, it is necessary to know the polymer conformation in the flow. The conformation of polymers, such as the unperturbed coil regime, trumpet regime, stem-and-flower regime, or extended state, was determined by the index φ . To estimate the polymer conformation, the index φ was calculated using the following procedure.

The force fN , which is required for calculating φ , acting on a single polymer was derived using eqn (2) and (3).

$$\Delta FL = \left(\sum_{i=1}^n f l_i \times \cos \alpha \right) \times 2 \times \cos \theta \quad (2)$$

$$\sum_{i=1}^n f l_i \times \cos \alpha = f \times \Delta l \times \frac{1}{2} n(n-1) \times \cos \alpha \quad (3)$$

Here, L m is the length of the cantilever beam, that is, $100 \mu\text{m}$, as shown in Fig. 6(a). The left term of eqn (2) indicates the torque applied to the cantilever, which equals the summation of the torque from each single polymer attached to the probe. As shown in Fig. 6, n – is the number of bonded polymers in a line along the hypotenuse of the V-shaped probe, which was calculated based on the grafting distance, Δl . Here, only the polymers attached to the edge of the V-shaped probe were considered. This is because the laminar boundary layer develops from the front edge of the oblique side of the probe, as

shown in Fig. 6(c). The boundary layer on the wall of the probe was much thicker than the polymer sizes.⁵¹ Therefore, only the mPEG-SH attached at the edge was subjected to flow and considered in the calculation. In addition, l_i m is the length between the upper edge of the probe and the position where the polymer is attached. The angle θ is the tilt angle of the cantilever, and the angle α is half the apex angle. Here, the grafting distance, Δl , was calculated based on data obtained from previous studies; Δl of mPEG-SH10k, mPEG-SH20k, and mPEG-SH40k were 2.5, 3.9, and 4.9 nm, respectively.^{51,52} The index φ of mPEG-SH calculated by f was varied from 0.015 to 0.1. Here, the persistent length l_{op} in the calculation of φ was referred to a previous study, which is $3.8 \times 10^{-10} \text{ m}$.⁵⁴ The value of φ suggests that the mPEG-SH attached to the cantilever probe did not reach an extended state only by the force applied in the flow. However, the conformation of polymers densely grafted on a surface tends to be stretched.⁵² Therefore, the stem and ellipsoidal-flower shape was proposed as a mPEG-SH conformation to calculate the contribution of each polymer molecule to the flow on ΔF —see Fig. 7(a) and (b).⁵¹

As shown in Fig. 7(a) and (b), to estimate the polymer conformation, the number of monomers in the stem part, N_{stem} , and that in the ellipsoidal-flower part, N_{flower} , must be calculated. Therefore, the force balance between the stem and ellipsoidal-flower parts was examined. Here, the sum of N_{stem} and N_{flower} is the total number of monomers, N_{total} , in a single mPEG-SH. The force owing to the stem part, F_{WLC} N, was calculated using the WLC model. The model described in eqn (4) is used to calculate the force required to stretch a single polymer chain.^{22,25,27}

$$F_{\text{WLC}} = \frac{k_B T}{l_{\text{op}}} \left[\frac{1}{4(1-x/L_{\text{total}})} + \frac{x}{L_{\text{total}}} - \frac{1}{4} \right] \quad (4)$$

where l_{op} is the persistent length, which is the same as in the calculation, φ , x m is the extension length, and L_{total} m is the contour length. Here, $x = N_{\text{stem}} \times l_{\text{op}}$, and $L_{\text{total}} = N_{\text{total}} \times l_{\text{op}}$. The force resulting from the ellipsoidal-flower part, F_{Stokes} N,

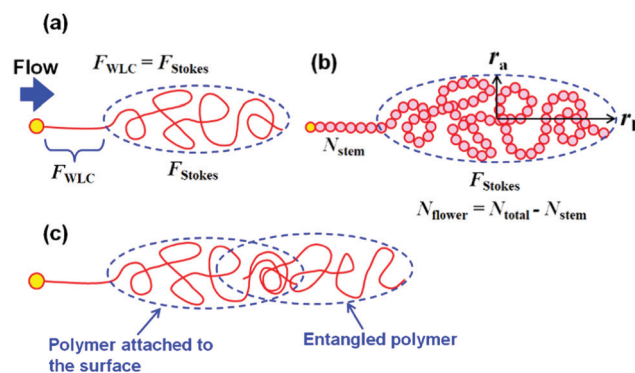


Fig. 7 (a) Force balance between the stem part and the ellipsoidal-flower part in a flow, (b) close-up figure of the polymer, focusing on the number of monomers, and (c) schematic of polymer entanglement in a flow; a polymer in a flow is entangled with a polymer attached to the gold-coated surface.

was calculated using the Stokes drag model of the ellipsoid:^{55,56}

$$F_{\text{Stokes}} = 6\pi\eta r_a \left\{ 1 - \frac{1}{5} \left(1 - \frac{r_b}{r_a} \right) \right\} V \quad (5)$$

Here, r_a m and r_b m are the radii of the minor and major axes of the ellipsoidal-flower part, respectively—see Fig. 7(b). Moreover, r_a was assumed to be half the length of the grafting distance, which is a constant value. To keep the stem and ellipsoidal-flower shape of a polymer molecule in the flow steadily, F_{WLC} and F_{Stokes} should be balanced. Therefore, the force balance between F_{WLC} and F_{Stokes} was used to obtain r_b at each velocity and solution viscosity. In the calculations, r_a was fixed at half the length of the grafting distance, and r_b was gradually varied to minimize the difference between F_{WLC} and F_{Stokes} . Then, r_b was used to calculate the number of monomers in the ellipsoidal-flower part by $r_b = a(N_{\text{flower}})^{3/5}$, where a m = 3.8×10^{-10} m is the diameter of a monomer in PEG. The number of monomers in the stem part was also obtained by $N_{\text{stem}} = N_{\text{total}} - N_{\text{flower}}$. Indeed, most of the monomers in a single polymer chain are in the ellipsoidal-flower part. Thus, it can be concluded that it was only the ellipsoidal-flower part that was mainly subjected to the flow contributed to the increase in the drag force. Consequently, the drag force, F_{Stokes} , caused by the ellipsoidal-flower part was considered a contribution of a single polymer chain, $f_{\text{single}} N$, as $f_{\text{single}} = F_{\text{Stokes}}$. Finally, eqn (6) was derived to compare the experimentally obtained value ΔF to the value calculated by the drag force of the polymer chains attached to the probe edge. In addition, eqn (7) was derived by combining eqn (6) with eqn (3) and (5) to clarify the relationship between ΔF and V . As summarized in eqn (7), our model simply describes the effects of velocity and polymer conformation on the increase of F without any fitting parameter.

$$\Delta F = \frac{\left(\sum_{i=1}^n f_{\text{single}} l_i \times \cos\alpha \right) \times 2 \times \cos\theta}{L} \quad (6)$$

$$\Delta F = A \times V, \quad (7)$$

$$A = \frac{6\pi\eta r_a \left\{ 1 - \frac{1}{5} \left(1 - \frac{r_b}{r_a} \right) \right\} \times \Delta l \times n(n-1) \times \cos\alpha \times \cos\theta}{L}$$

Fig. 8 shows the comparison described in eqn (7), which was applied to the increase in force, ΔF , in the flows of glycerol solutions. Here, ΔF was calculated by comparing the forces measured by a naked cantilever and by a mPEG-SH-bonded cantilever. The molecular weight of mPEG-SH was varied from 10k to 40k, and the concentration of the glycerol solution was varied from 5 to 35 wt%. The open symbols show the experimental values with error bars, and the solid lines show the calculated values obtained using eqn (7). The experimental and calculated values are similar for each glycerol solution and for each molecular weight of mPEG-SH. Therefore, the assumption of the polymer conformation as a stem and ellipsoidal-flower model and

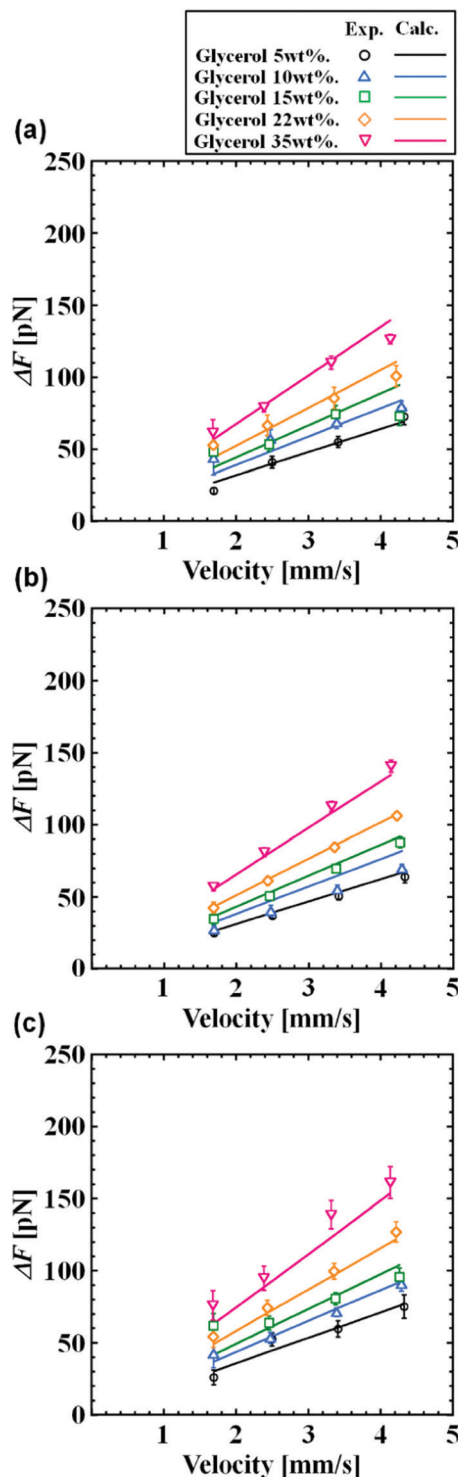


Fig. 8 Comparison of the experimentally obtained ΔF (Exp.) and the value obtained by eqn (7) (Calc.) in the flows of glycerol solutions. The molecular weights of mPEG-SH attached to the cantilever probe were (a) 10k, (b) 20k, and (c) 40k.

the drag force calculated by the Stokes drag of the ellipsoidal flower was more generalized for several molecular weights of mPEG-SH.

However, in the case of ΔF —comparing the force measured by a naked cantilever and by a mPEG-SH-bonded cantilever in

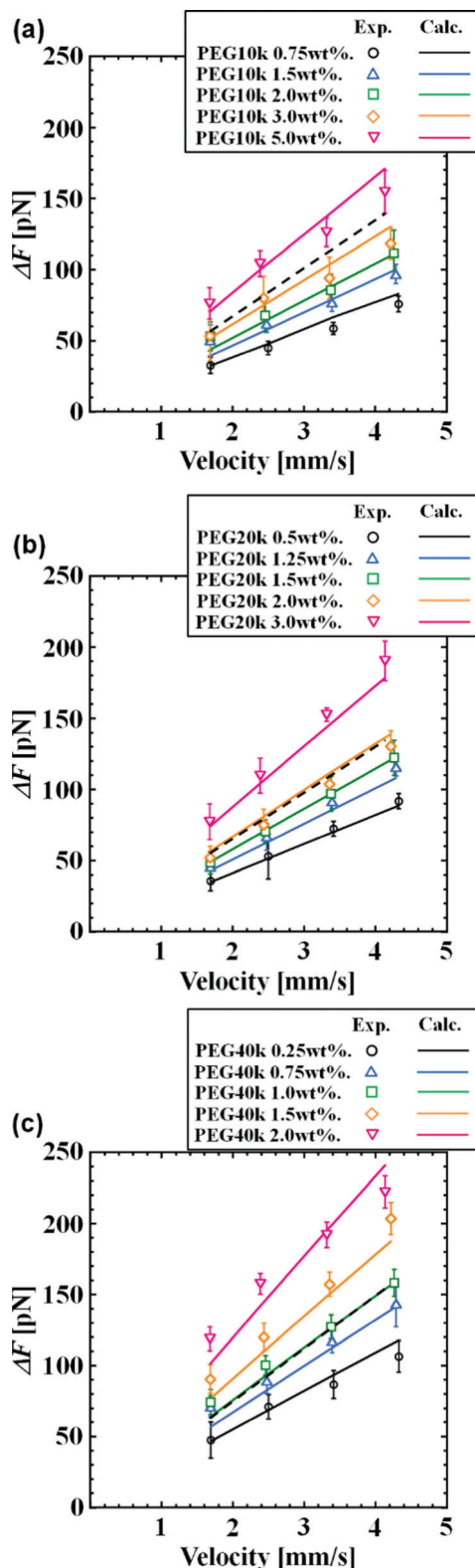


Fig. 9 Comparison of the experimentally obtained ΔF (Exp.) and the value obtained using eqn (7) (Calc.) in the flow of PEG solutions. The molecular weights of mPEG-SH attached to the cantilever probe were (a) 10k, (b) 20k, and (c) 40k. The black dotted-line in the figure shows the value of calculated ΔF without entanglement in (a) PEG 10k 5.0 wt%, (b) PEG 20k 3.0 wt% and (c) PEG 40k 2.0 wt% solutions.

the flow of PEG solutions—the increase was larger than that in the flow of glycerol solutions. Thus, the assumption of the stem and ellipsoidal-flower model for a single chain to calculate the drag force based on the velocity around the polymer chain and the viscosity of the solution did not fit well. It is considered that the increase resulted from polymer-polymer interaction in the flow: for instance, PEG molecules in the flow were caught by mPEG-SH attached to the probe, as shown in Fig. 7(c). Although PEG solutions flowing in the channel were categorized in dilute or semi-dilute unentangled regime, the cantilever was subjected to the flow, and the PEG solutions continued to flow. Therefore, polymers in the flow may entangle or attach to the polymers grafted on the cantilever. Here, it is assumed that PEG in the flow was entangled with the mPEG-SH on the probe, and the Stokes drag from these polymers was calculated. To calculate the drag force of polymers, *i.e.*, the mPEG-SH entangled with PEG, as shown in Fig. 7(c), the molecular weight of PEG was added to that of mPEG-SH as if a larger molecular weight of mPEG-SH were attached to the probe. The cantilevers with mPEG-SH10k, mPEG-SH20k, and mPEG-SH40k were immersed in the flow of PEG10k, PEG20k, and PEG35k solutions, respectively. The difference in ΔF measured in PEG solutions became larger when the molecular weight of mPEG-SH attached to the probe and PEG in the flows was higher (see Fig. 5 and 9). To describe the increase in ΔF depending on the molecular weight of mPEG-SHs and PEGs, the number of entangled polymers was varied. The 0.6 PEG10k chain on average was entangled with mPEG-SH10k, a single PEG20k chain on average was entangled with the mPEG-SH20k, and two PEG35k chains on average were entangled with mPEG-SH40k. Although the assumption was simple, the model illustrated in Fig. 7(c) describes the experimental data well, as shown in Fig. 9. Therefore, the stem and ellipsoidal-flower model with the assumption of polymer entanglement was considered reasonable for explaining the increase in drag force caused by polymers in the flow of the polymer solution. This model should be useful for describing polymer-fluid and polymer-polymer interactions in a flow. Because such small-scale interactions affect fluid behavior on a larger scale, the model proposed in this study can elucidate the complex behaviors of polymer solutions, which will be considered in future work.

4. Conclusions

The drag force of mPEG-SH with several molecular weights was measured in flows of glycerol and PEG solutions. The drag force was affected by the molecular weights of mPEG-SH attached to the cantilever probe, the solute, and the molecular weight of the PEGs in the flows. The stem and ellipsoidal-flower model proposed in a previous study⁵¹ was adapted to describe the drag force. The model fitted well to the drag force of mPEG-SH with any molecular weight in glycerol solution flows. However, the drag force measured in the flow of the PEG solutions deviated from the model. This was attributed to the polymer-polymer interaction in flows between mPEG-SH attached to the

probe and PEGs in the flow. To describe the polymer–polymer interaction, the entanglement of polymers with mPEG–SH attached to the probe was considered in the calculation. The drag force calculated by the stem and ellipsoidal-flower model containing the increase in the force resulting from polymer entanglement fit the experimental value well. The model assumption was simple, but it described the drag force of polymers well. Polymer deformations, entanglements, and the force caused by these polymers in the near-wall region affect the flows of non-Newtonian fluids. Therefore, the polymer drag force prediction based on a simple model is deemed promising.

Conflicts of interest

There are no conflicts to declare.

Acknowledgements

The present study was supported in part by a Grant-in-Aid for Scientific Research (B) (Project No. 19H02497) from the Japan Society for the Promotion of Science (JSPS KAKENHI) and by the Fusion-Oriented-Research-for-disruptive-Science-and-Technology (FOREST) initiative from the Japan Science and Technology Agency.

Notes and references

- M. D. Graham, *Phys. Fluids*, 2014, **26**, 101301.
- B. E. Owolabi, D. J. C. Dennis and R. J. Poole, *J. Fluid Mech.*, 2017, **827**, R4.
- R. Hidema, I. Murao, Y. Komoda and H. Suzuki, *J. Non-Newtonian Fluid Mech.*, 2018, **254**, 1.
- R. Hidema, K. Fukushima, R. Yoshida and H. Suzuki, *J. Non-Newtonian Fluid Mech.*, 2020, **285**, 104385.
- L. E. Rodd, T. P. Scott, D. V. Boger, J. J. Cooper-White and G. H. McKinley, *J. Non-Newtonian Fluid Mech.*, 2005, **129**, 1.
- R. Hidema, T. Oka, Y. Komoda and H. Suzuki, *Phys. Fluids*, 2019, **31**, 072005.
- C. M. Schroeder, *J. Rheol.*, 2018, **62**, 371.
- T. T. Perkins, D. E. Smith and S. Chu, *Science*, 1997, **276**, 2016.
- D. E. Smith, H. P. Babcock and S. Chu, *Science*, 1999, **283**, 1724.
- K. D. Dorfman, S. B. King, D. W. Olson, J. D. P. Thomas and D. R. Tree, *Chem. Rev.*, 2013, **113**, 2584.
- S. J. Haward, A. Jaishankar, M. S. N. Oliveira, M. A. Alves and G. H. McKinley, *Biomechanics*, 2013, **7**, 044108.
- F. J. Galindo-Rosales, M. S. N. Oliveira and M. A. Alves, *RSC Adv.*, 2014, **4**, 7799.
- Y. Liu, K. Zografos, J. Fidalgo, C. Duchêne, C. Quintard, T. Darnige, V. Filipe, S. Huille, O. du Roure, M. S. N. Oliveira and A. Lindner, *Soft Matter*, 2020, **16**, 9844.
- K. Zografos, S. J. Haward and M. S. N. Oliveira, *Microfluid. Nanofluid.*, 2019, **23**, 131.
- D. Dohi, K. Hirano and K. Terao, *Biomechanics*, 2020, **14**, 014115.
- A. Masuda, H. Takao, F. Shimokawa and K. Terao, *Sci. Rep.*, 2021, **11**, 7961.
- D. W. Trahan and P. S. Doyle, *Biomechanics*, 2009, **3**, 012803.
- A. Balducci and P. S. Doyle, *Macromolecules*, 2008, **41**, 5485.
- C. Ortiz and G. Hadziioannou, *Macromolecules*, 1999, **32**, 780.
- M. Rief, M. Gautel, F. Oesterhelt, J. M. Fernandez and H. E. Gaub, *Science*, 1997, **275**, 1295.
- F. Oesterhelt, M. Rief and H. E. Gaub, *New J. Phys.*, 1999, **1**, 6.
- K. Nakajima and T. Nishi, *Chem. Rec.*, 2006, **6**, 249.
- F. Kienberger, V. Ph. Pastushenko, G. Kada, H. J. Gruber, C. Riener, H. Schindler and P. Hinterdorfer, *Single Mol.*, 2000, **1**, 123.
- C. Bustamante, *Science*, 1994, **265**, 1599.
- X. Liang and K. Nakajima, *Macromol. Chem. Phys.*, 2018, **219**, 1700394.
- N. Maman, P. Kumar, A. Yadav and M. Feingold, *Front. Mol. Biosci.*, 2021, **8**, 609076.
- M. I. Giannotti and G. J. Vancso, *ChemPhysChem*, 2007, **8**, 2290.
- M. Hinczewski and R. R. Netz, *Macromolecules*, 2011, **44**, 6972.
- B. J. Haupt, T. J. Senden and E. M. Sevick, *Langmuir*, 2002, **18**, 2174.
- M. S. Z. Kellermayer, S. B. Smith, H. L. Granzier and C. Bustamante, *Science*, 1997, **276**, 1109.
- Z. N. Scholl, Q. Li and P. E. Marszalek, *Wiley Interdiscip. Rev.: Nanomed. Nanobiotechnol.*, 2014, **6**, 211.
- N. B. Holland, T. Hugel, G. Neuert, A. Cattani-Scholz, C. Renner, D. Oesterhelt, L. Moroder, M. Seitz and H. E. Gaub, *Macromolecules*, 2003, **36**, 2015.
- M. I. Giannotti, I. Cabeza de Vaca, J. M. Artés, F. Sanz, V. Guallar and P. Gorostiza, *J. Phys. Chem.*, 2015, **119**, 12050.
- T. T. Perkins, D. E. Smith, R. G. Larson and S. Chu, *Science*, 1995, **83**, 268.
- J. F. Marko and E. D. Siggia, *Macromolecules*, 1995, **28**, 8759.
- T. Saito, T. Sakaue, D. Kaneko, M. Washizu and H. Oana, *J. Chem. Phys.*, 2011, **135**, 154901.
- H. Wang and J. E. Pemberton, *Langmuir*, 2017, **33**, 7468.
- H. Wang and J. E. Pemberton, *Langmuir*, 2019, **35**, 13646.
- J. L. Harden and M. E. Cates, *Phys. Rev. E*, 1996, **53**, 3782.
- P.-Y. Lai and C.-Y. Lai, *Phys. Rev. E*, 1996, **54**, 6958.
- S. Ji and J. Dinga, *J. Chem. Phys.*, 2005, **123**, 144904.
- B. Ladoux and P. S. Doyle, *Europhys. Lett.*, 2000, **52**, 511.
- J. K. Fisher, M. Ballenger, E. T. O'Brien, J. Haase, R. Superfine and K. Bloom, *Proc. Natl. Acad. Sci. U. S. A.*, 2009, **106**, 9250.
- T. Roy, K. Szuttor, J. Smiatek, C. Holm and S. Hardt, *Soft Matter*, 2017, **13**, 6189.
- F. Brochard-Wyart, *Europhys. Lett.*, 1993, **23**, 105.
- F. Brochard-Wyart, H. Hervet and P. Pincus, *Europhys. Lett.*, 1994, **26**, 511.

- 47 F. Brochard-Wyart, *Europhys. Lett.*, 1995, **30**, 387.
- 48 A. Buguin and F. Brochard-Wyart, *Europhys. Lett.*, 1996, **29**, 4937.
- 49 F. Brochard-Wyart, A. Buguin and P. G. de Gennes, *Europhys. Lett.*, 1999, **47**, 171.
- 50 R. Rzehak, W. Kromen, T. Kawakatsu and W. Zimmermann, *Eur. Phys. J. E: Soft Matter Biol. Phys.*, 2000, **2**, 3.
- 51 R. Hidema, S. Hayashi and H. Suzuki, *Phys. Rev. Fluids*, 2019, **4**, 074201.
- 52 R. L. Schoch and R. Y. H. Lim, *Langmuir*, 2013, **29**, 4068.
- 53 R. K. Shah and A. L. London, *Laminar forced convection in ducts*, Academic Press, 1978.
- 54 H. Lee, R. M. Venable, A. D. MacKerellJr and R. W. Pastor, *Biophys. J.*, 2008, **95**, 1590.
- 55 Y. Magariyama, S. Sugiyama, K. Muramoto, I. Kawagishi, Y. Imae and S. Kudo, *Biophys. J.*, 1995, **69**, 2154.
- 56 J. Happel and H. Brenner, *Low Reynolds number hydrodynamics*, Springer, 1983.